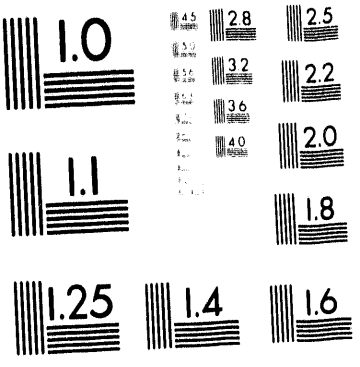
1.0
2.8
2.5
3.2
2.2
3.6
4.0
2.0
1.1
1.8
1.25
1.4
1.6

1 of 1

Spectroscopic Observation of 0-300 keV ^{3}He Ions Produced by ICRF Heating in the TFTR Tokamak

B. C. Stratton, R. J. Fonck*, G. McKee*, T. Thorson*,
G. Hammett, C. K. Phillips, and E. J. Synakowski

Princeton Plasma Physics Laboratory, Princeton University,
P. O. Box 451, Princeton, NJ 08543

*Department of Nuclear Engineering and Engineering Physics,
University of Wisconsin, Madison, WI 53706

ABSTRACT

^{3}He ions with energies from thermal values up to 300 keV produced by ICRF heating have been spectroscopically observed by the α-CHERS diagnostic on TFTR. The shape of the spectrum and the temporal and spatial behavior of the energetic ^{3}He ion emission are consistent with expectations for this ICRF heating case. Because the ^{3}He ion density was similar to the alpha particle density predicted for D-T supershots on TFTR, these observations give confidence that confined alphas produced by D-T fusion reactions can be observed by α-CHERS during D-T operation of TFTR.

MASTER

DISTRIBUTION OF THIS DOCUMENT IS UNLIMITED

A major goal of deuterium-tritum (D-T) operation of the Tokamak Fusion Test Reactor (TFTR) is to study the physics of confined nonthermal alpha particles produced by D-T fusion reactions. Measurements of the spatial and velocity distributions of alphas as they slow down from their birth energy of 3.5 MeV to thermal energies will be important to understanding alpha physics and, thus, to predicting alpha behavior in future devices such as ITER. To help achieve this goal, several confined alpha diagnostics have been implemented on the TFTR tokamak. One such diagnostic is the Alpha Charge Exchange Recombination Spectroscopy experiment (α-CHERS) [1,2], which will observe confined alphas with energies from thermal values to an upper limit of 0.5-1.0 MeV.

Because α-CHERS is the first implementation of a new measurement technique for D-T alphas, it was desirable to evaluate its capabilities prior to D-T operation of TFTR by performing an experiment to observe a simulated population of energetic alphas. This letter presents the results of such an experiment: ^{3}He ions with energies up to 300 keV produced by ICRF heating were observed by the prototype α-CHERS system. The ^{3}He ion density was similar to the alpha density expected for high-Q D-T discharges on TFTR, although the velocity distribution produced by RF heating is anisotropic, while that of the D-T alphas is expected to be close to isotropic. The time evolution and spatial profiles of the energetic ^{3}He ion emission are consistent with expectations for this ICRF heating case, and the shape of the observed spectrum is very similar to that predicted from a Fokker-Planck calculation of the ^{3}He ion distribution function for this case. Thus, this experiment provides confidence that the D-T alpha signal on TFTR can be observed. In a similar vein, ^{3}He ions from a 135 keV helium neutral beam have been observed on the JET tokamak by charge exchange recombination spectroscopy, albeit at a higher helium ion density [3].

The concepts of charge exchange recombination spectroscopy of alpha particles were originally discussed by Post, *et al.* [4], and most recently by von Hellermann, *et al.* [3]. Post *et al.* [5] proposed utilizing energetic ^{3}He ions produced by ICRF heating to simulate fusion alphas. The α-CHERS signal is due to reactions in which charge exchange takes place during a collision between an alpha and an energetic deuterium atom injected by a neutral beam, leaving a He^+ ion in an excited level with principal quantum number n=4, which then decays to level n=3 by emitting line radiation at 468.6 nm. α-CHERS views the deuterium heating neutral beams which are injected tangentially and operated at an energy of 95 keV in this experiment. The cross section for excitation of this line is strongly peaked at low relative velocity (approximately 30 keV/amu), and the observed emission is therefore primarily from ions with a narrow range of velocities near the beam velocity. As a result, the spectral line shape is determined by the angle between the beam and the spectrometer sightline, φ, and the emission from the nonthermal particles appears as broad wings on the thermal line emission. For $\varphi \neq 90°$, the wings are asymmetric around the thermal 468.6 nm line. The α-CHERS sightlines on TFTR were chosen to produce a red shift of the energetic alpha emission to avoid

strong lines of low ionization states of carbon present on the short wavelength side of the He^+ 468.6 nm line.

Predictions of the α-CHERS signal for D-T plasmas show that while the line wing is weak compared to the bremsstrahlung background, measurements with a useful signal-to-noise ratio can be obtained by a high throughput optical system in which the detector noise is dominated by photon statistics [1,2]. Thus, the prototype α-CHERS instrumentation consisted of high-throughput input optics and spectrometers coupled to low-noise charge-coupled-device (CCD) cameras. The instrumentation used in the present experiment is described only briefly here; details may be found in references 1 and 2. Following the completion of this work, the α-CHERS hardware was upgraded to allow simultaneous observation of six spatial points for D-T operation of TFTR.

A tangential array of sightlines in the torus midplane was used to view three co-injected neutral beams. This array has five spatial channels and radial resolution of 0.02 m, with φ=43.7° for the sightline intersecting the beams at a major radius of 3.08 m. A schematic diagram of the sightlines and beams is shown in Fig. 1. Light from a selected spatial channel is coupled via optical fibers to a 0.275 m Czerny-Turner spectrometer with 1.0 nm spectral resolution. The spatial channel viewed by the spectrometer can be selected between shots; thus, a five point spatial scan can be performed by combining data from five reproducible shots. The detector is a low-noise, back-illuminated, 512 × 512 pixel CCD camera. The camera was not shuttered during readout, so the time resolution was determined by the readout time, which was 0.1 s in this experiment. Statistical analysis of the noise on the data demonstrates that it is very close to that predicted by photon statistics. To correct for pixel-to-pixel variations in the gain of the detector, a flat field correction was applied to the data. The background signal in the absence of light was measured before each shot and was subtracted from each readout of the camera (frame) of data taken during the discharge.

To produce a significant nonthermal ^3He ion distribution under conditions similar to those expected for D-T operation, a moderate density discharge with $\bar{n}_e = 2.6 \times 10^{19}\ m^{-3}$ was used in this experiment. This was accomplished by injecting 3 co-directed neutral beams and 3 counter-beams (where co- and counter are defined as the directions parallel and anti-parallel to the plasma current), for a total beam power of 14 MW. The time evolutions of $\bar{n}_e$, the beam power, and the RF power are shown in Fig. 2 for a case with 4.0 MW RF power. The duration of the beam pulse was 2 s; the RF pulse was 1 s long, starting 0.5 s into the beam pulse and ending 0.5 s before the end of the beam pulse. This timing was chosen to allow $\bar{n}_e$ to reach a nearly steady state value before the start of the RF pulse and to allow the signal during the RF pulse to be compared with the signal following the RF pulse, with the beams on at both times. A ^3He puff of 0.1 s duration was introduced starting at 2.3 s; the ^3He concentration was measured from the n_e rise to be 1.5% of $n_e(0)$, equivalent to a density of $6.0 \times 10^{17}\ m^{-3}$ on axis. Larger ^3He concentrations produce lower average ^3He ion energies for a given RF power, so it was not

possible to increase the α-CHERS signal by increasing the ^{3}He concentration. The plasma current in these discharges was 1.4 MA and the toroidal field was 4.8 T. The major and minor radii were R=2.62 m and a=0.97 m, respectively.

The α-CHERS spectrum from one frame of data near the end of the 4.0 MW RF pulse is shown in Fig. 3. This spectrum is from a sightline which intersects the neutral beams at R=3.08 m (r/a=0.3), the spatial location at which the largest signal was seen. The thermal He^+ 468.6 nm line is present along with a number of other impurity lines and the background bremsstrahlung continuum. The emission from energetic ^{3}He ions is present as a broad wing on the long wavelength side of the thermal He^+ line.

The line wing is more clearly seen in Fig. 4, which shows data from the same shot at three different times: immediately before the start of the RF pulse, at the beginning of the RF pulse, and near the end of the RF pulse. A constant value of the bremsstrahlung background evaluated at 476.4 nm (equivalent ^{3}He ion energy=390 keV) for each time point was subtracted, and the signals were normalized to each other at this wavelength to show more clearly the change in the shape of the line wing. To illustrate the range of ^{3}He ion energies observed, the spectra are plotted as a function of ^{3}He ion energy determined from the measured Doppler shift. (The energy is derived from the ^{3}He ion velocity along the sightline, which is close to the velocity along the field lines for this viewing geometry.) It is clear that emission from ^{3}He ions with energies up to 300 keV is present in the spectrum. The enhancement of the line wing at the start of the RF pulse is small because the population of energetic ^{3}He ions is not yet fully developed, while the line wing at the end of the RF pulse is much stronger because a steady state population of energetic ions has been established by this time.

Fig. 5 shows a predicted energetic ^{3}He ion spectrum compared with the measured spectrum at the end of the RF pulse. The predicted spectrum is based on the ^{3}He ion distribution function calculated for this discharge by the FPP/SPRUCE code [6,7], which solves the bounce-averaged Fokker-Planck equation to find the fast ion distribution function as a function of energy, pitch angle, and radius in the plasma midplane. FPP [6] includes the bounce-averaged quasilinear RF-heating operator and the collisional thermalization operator. SPRUCE [7] solves the 3-dimensional wave equation for the ICRF fast wave, incorporating propagation, focusing, diffraction, and damping. The effects of fundamental and second harmonic ion damping, electron damping, and mode conversion are included. The distribution function at the appropriate radius and pitch angle was normalized to the measured value of the ^{3}He density and was used to calculate the spectrum. The line excitation cross sections used were those of von Hellermann, *et al.* [8] with full l-mixing, and the beam atom density was calculated including the effects of excitation before ionization [9]. The shape of the thermal line wing is determined primarily by the instrument function; it was modeled by a Gaussian whose width and amplitude were adjusted to reproduce the line wing before the RF pulse (the spectrum at time T_1 in Fig. 4). This procedure is expected to accurately reproduce the thermal

line wing at the end of the RF pulse because T_i at R=3.08 m increased from 9 keV to 11 keV during the RF pulse, resulting in a small increase in the line width compared to the instrumental width. Comparison of the curves in Fig. 5 shows that the observed and calculated energetic ^{3}He ion spectra have a very similar shape. In future measurements of D-T alphas, absolute calibration of α-CHERS will make it possible to derive the absolute alpha density from the data.

Fig. 6 shows the time evolution of the energetic ^{3}He ion signal obtained by integrating the difference between the total signal and the bremsstrahlung contribution over the spectral range corresponding to the energy range 40-270 keV for each frame. The signal at lower energies was excluded to minimize the contribution of the thermal line. Also shown is the signal from a similar shot with P_{RF}=0. The increase in the signal at the onset of beam injection is due to the broadening of the line wing caused by the increase in T_i at R=3.08 m from 2 keV to 9 keV and is similar for the two cases. An increase in the signal is seen early in the RF pulse. The signal remains roughly constant until the end of the RF pulse, and then it decays to the pre-RF level in approximately 0.3 s. (In the P_{RF}=0 comparison shot, the beam pulse ended at 4.0 s, resulting in different time evolutions of the signals after this time.) Thus, the intensity of the energetic ^{3}He ion emission is well correlated in time with the RF pulse, and the finite time required for the signal to decay following the end of the RF pulse is comparable to the calculated slowing down time of 0.1 s in this discharge.

A five-point radial profile of the energetic ^{3}He ion emission is shown in Fig. 7. This scan was performed on a shot-to-shot basis at P_{RF}=2.6 MW, the highest power at which reliable RF operation could be obtained. For each spatial point, the signal was integrated over the ^{3}He ion energy range 40-270 keV and the bremsstrahlung background was subtracted. The signal was averaged over the later half of the RF pulse (3.5-4.0 s) and the signal following the RF pulse, but before the end of beam injection (4.4 s), was subtracted to remove the contributions of weak edge impurity lines. (The energetic ^{3}He ion line wing was not observable in the outermost spatial channel at R=3.50 m and the signal was dominated by edge lines, so the signal at this radius was set to zero in Fig. 7.) The signal was normalized to the calculated beam atom density, resulting in a quantity proportional to the total energetic ^{3}He ion density at a given radius. The magnetic axis in this discharge was located at R=2.85 m, and FPP/SPRUCE code [6,7] modeling for this case shows that the RF power deposition peaked at a minor radius of 0.15 m. As a result, the peak of the energetic ^{3}He ion density is expected to be at R=3.00 m. The energetic ion density was found to peak off-axis, as expected, but a radius of R=3.08 m, which is somewhat larger than predicted. However, this is acceptable agreement given this relatively simple analysis and that the radial profile consists of only 5 widely-spaced points.

In addition to prompt charge exchange, a source of signal is the plume of recombined $^3He^+$ ions that drift out of the beam volume along field lines and are excited by electron, proton, or impurity ion impact, radiating in the spectrometer field of view [10]. A crude calculation

shows that the plume emission is approximately 50% of the prompt charge exchange emission for the α-CHERS sightline intersecting the beams at R=3.08 m. This has the effect of spatially delocalizing the signal to some extent and may affect the line shape, especially at low energies. It is clear that more detailed experimental studies and modeling of the plume will be needed for quantitative interpretation of α-CHERS data in these and D-T discharges.

Finally, it is worthwhile to compare the intensity of the predicted ^{3}He signal shown in Fig. 5 with the predicted alpha signal for a D-T supershot on TFTR. The D-T alpha spectrum was calculated assuming an alpha density of 2×10^{17} m^{-3}, as predicted by TRANSP code simulations of the D-T performance of a supershot with Q_{DT}=0.23 at I_p=1.6 MA and 24 MW beam power [11]. This alpha density is smaller than the ^{3}He ion density observed in this experiment by approximately a factor of three. Classical slowing down of the alphas was assumed in the calculation of the spectrum, and the beam density was calculated from the parameters of the simulated D-T discharge. At an alpha energy of 300 keV, the predicted D-T alpha signal is smaller than the predicted RF ^{3}He ion signal shown in Fig. 5 by a factor of 5. Given planned improvements in the apparatus and the development of a full nonlinear modeling algorithm, it should be possible to extract nonthermal alpha signals considerably smaller than those observed here. This observation therefore provides confidence that the energetic alpha spectrum can be observed in D-T discharges on TFTR.

ACKNOWLEDGEMENTS

The authors would like to thank the TFTR ICRF group for their support of this experiment, R. Budny for useful discussions, and K. Young for his support of this project. This work was supported by U. S. Department of Energy Contract No. DE-AC02-76-CHO-3073 and Grant No. DE-FG02-89-ER53296.

REFERENCES

1. B. C. Stratton, R. J. Fonck, Y. J. Kim, G. McKee, and T. Thorson, Rev. Sci. Instrum. **63** (1992) 5179.
2. T. Thorson, G. McKee, R. J. Fonck, and B. Stratton, Rev. Sci. Instrum. **63** (1992) 5182.
3. M G. von Hellermann and H. P. Summers, Rev. Sci. Instrum. **63** (1992) 5132.
4. D. E. Post, *et al.*, J. Fusion Energy **1** (1981) 129.
5. D. E. Post, D. Hwang, D. Mikkelsen, and F. Seidl, J. Vac. Sci. Technol. A **1** (1983) 206.
6. G.W. Hammett, "Fast Ion Studies of Ion Cyclotron Heating in the PLT Tokamak", Ph. D. Dissertation (Princeton, 1986).
7. D. N. Smithe, P. L. Colestock, R. J. Kashuba, and T. Kammash, Nucl. Fusion **27** (1987) 1319.
8. M. von Hellermann, *et al.*, Plasma Phys. Controlled Fusion **33** (1991) 1805.
9. C. D. Boley, R. K. Janev, and D. E. Post, Phys. Rev. Lett. **52** (1984) 534.
10. R. J. Fonck, D. S. Darrow, and K. P. Jaehnig, Phys. Rev. A **29** (1984) 3288.
11. R. Budny, "A Standard DT Supershot Simulation", Princeton Plasma Physics Laboratory Report No. PPPL-2930 (Sept. 1993).

FIGURE CAPTIONS

Fig. 1: Schematic diagram of α-CHERS sightlines and neutral beam trajectories on TFTR.

Fig. 2: Time evolution of $\bar{n}_e$, total beam power, and RF power for the shot shown in Figs. 3-6. The times shown in Fig. 4 are indicated by arrows.

Fig. 3: α-CHERS spectrum at the end of the RF pulse (T_3=3.9 s in Fig. 2). The energetic ^{3}He ion emission is present as a broad wing on the long wavelength side of the thermal He^+ 468.6 nm line.

Fig. 4: α-CHERS spectra at the times indicated in Fig. 2, with wavelength converted to alpha energy using the measured Doppler shift of the emission. The bremsstrahlung background has been subtracted and the spectra have been normalized at 476.4 nm (equivalent ^{3}He ion energy=390 keV).

Fig. 5: α-CHERS spectrum predicted from the ^{3}He ion distribution function calculated by the FPP/SPRUCE code [6,7] compared with the measured spectrum at the end of the RF pulse.

Fig. 6: Time evolution of the intensity of the energetic ^{3}He ion line wing integrated over wavelengths corresponding to alpha energies of 40-270 keV, with the bremsstrahlung background subtracted. The signal from a shot with P_{RF}=0 is shown for comparison.

Fig. 7: Radial profile at P_{RF}=2.6 MW of the energetic ^{3}He ion emission integrated over the energy range 40-270 keV. The bremsstrahlung background and the signal following the RF pulse (4.4 s) have been subtracted. The signal has been normalized to the calculated beam atom density to yield a quantity proportional to the energetic ^{3}He ion density.

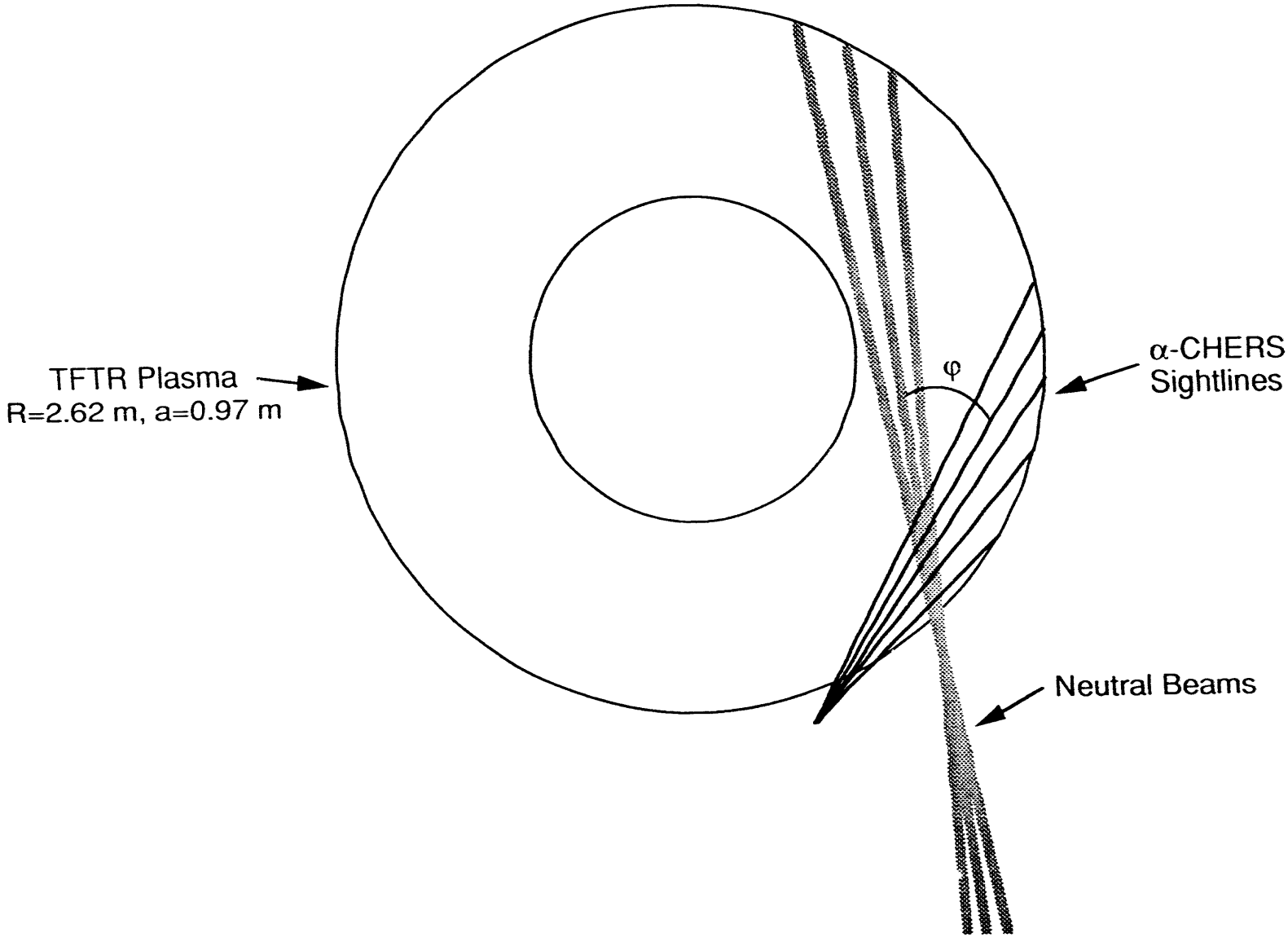

Fig. 1

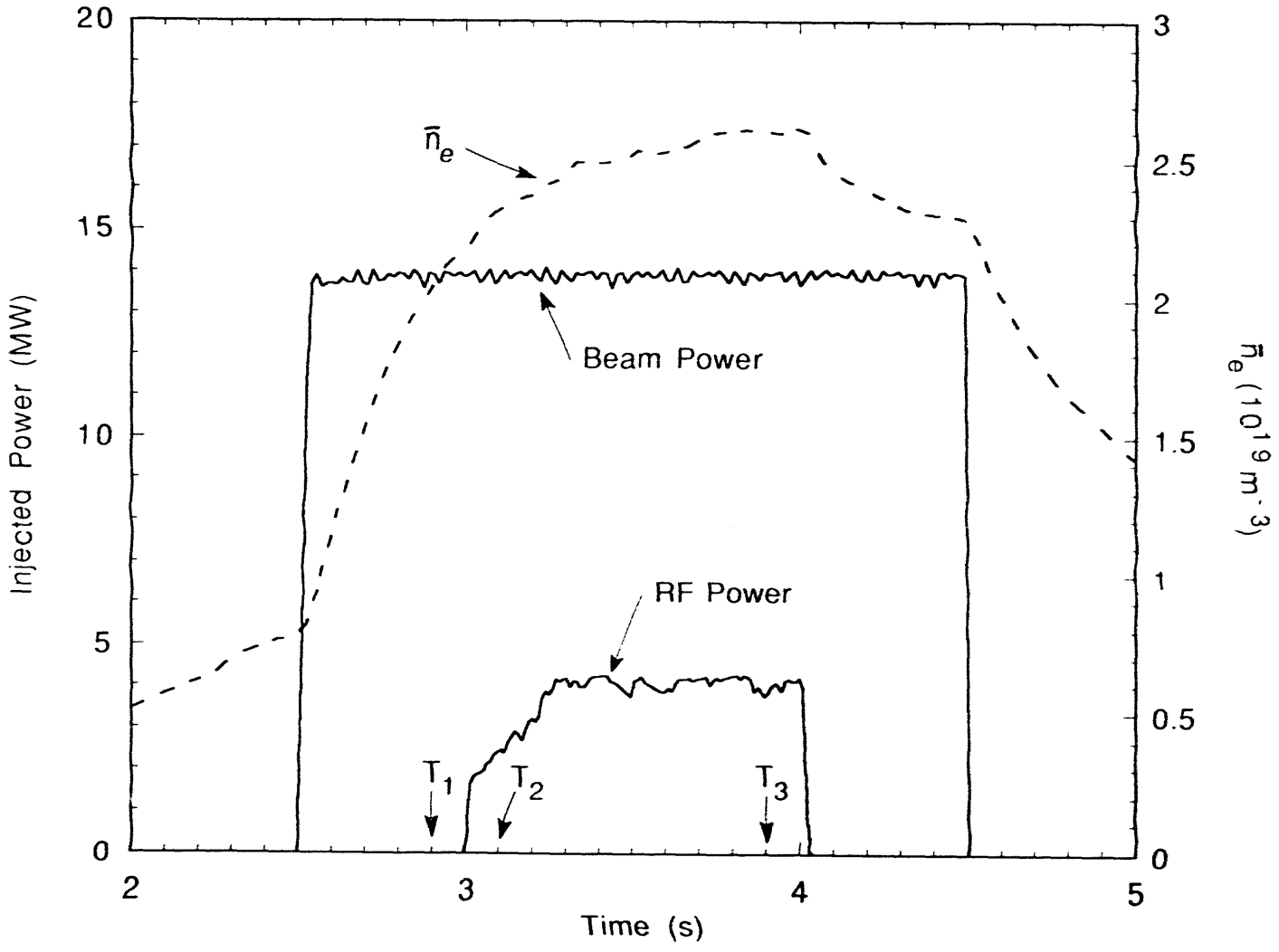
20
15
10
5
0
Injected Power (MW)
3
2.5
2
1.5
1
0.5
0
$\bar{n}_e$ (10^{19} m^{-3})
2
3
4
5
Time (s)
$\bar{n}_e$
Beam Power
RF Power
T_1
T_2
T_3

Fig. 2

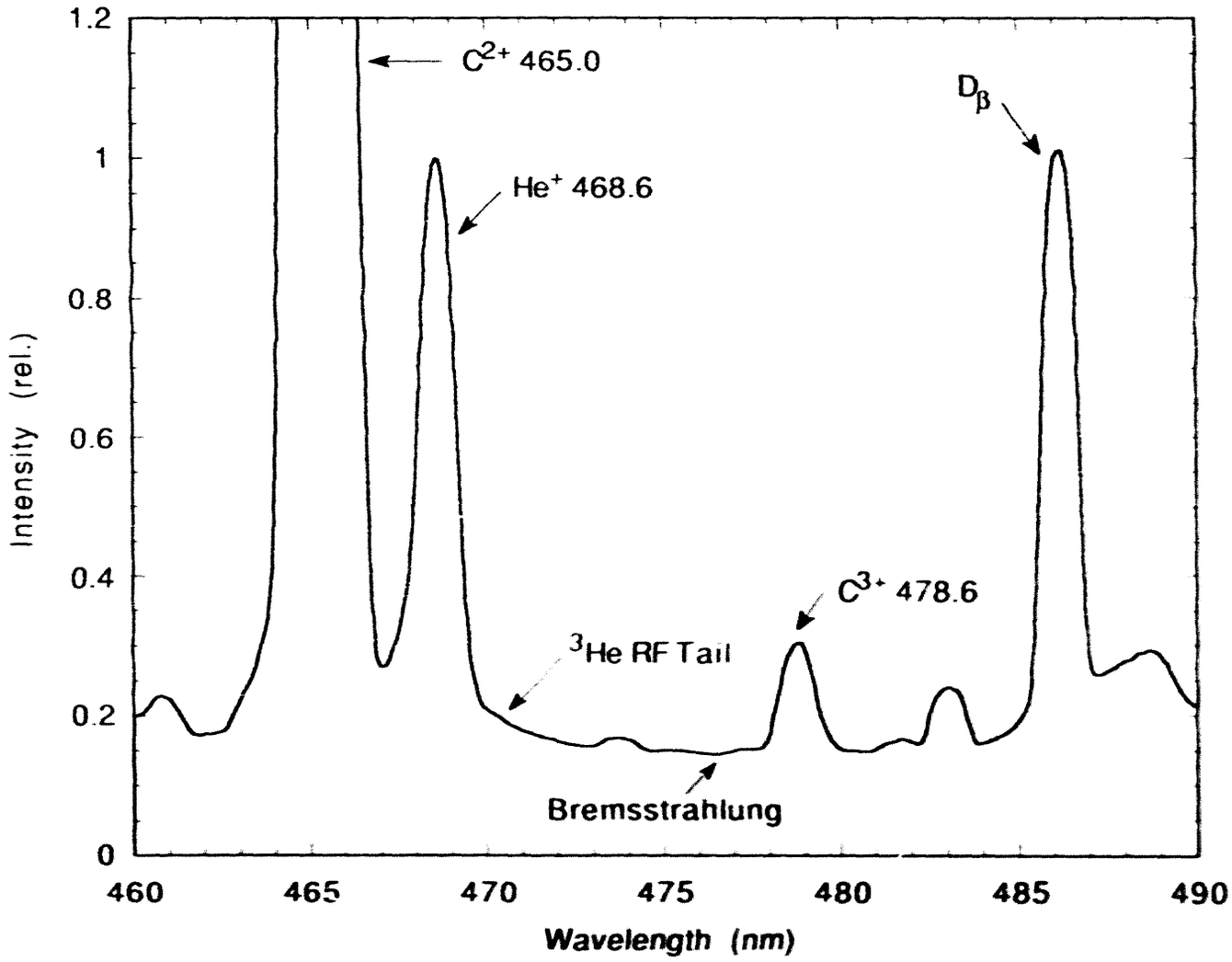
1.2
1
0.8
0.6
0.4
0.2
0
Intensity (rel.)
460
465
470
475
480
485
490
Wavelength (nm)
C2+ 465.0
He+ 468.6
Dβ
C3+ 478.6
3He RF Tail
Bremsstrahlung

Fig. 3

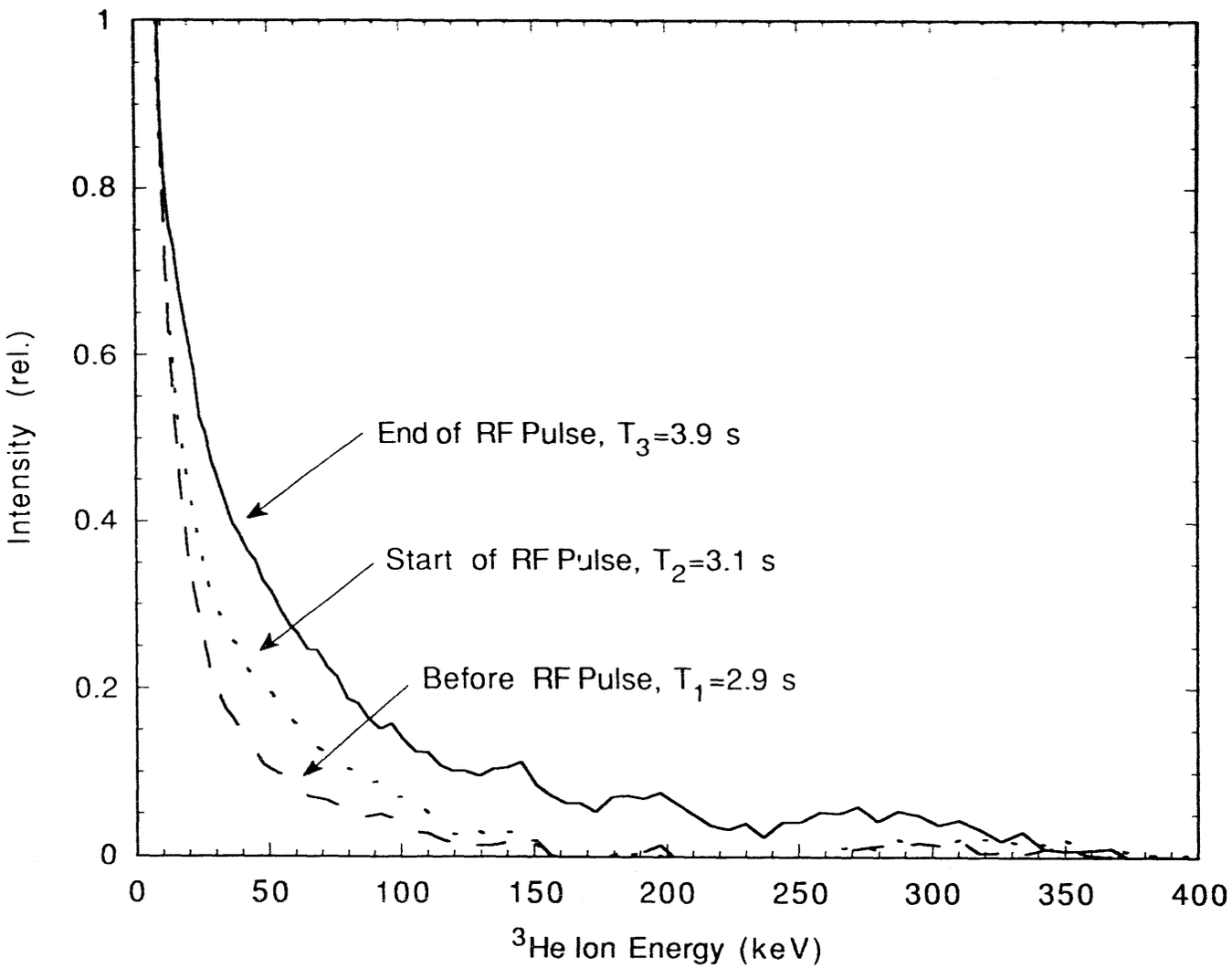
1
0.8
0.6
0.4
0.2
0
Intensity (rel.)
0
50
100
150
200
250
300
350
400
^{3}He Ion Energy (keV)
End of RF Pulse, T_3=3.9 s
Start of RF Pulse, T_2=3.1 s
Before RF Pulse, T_1=2.9 s

Fig. 4

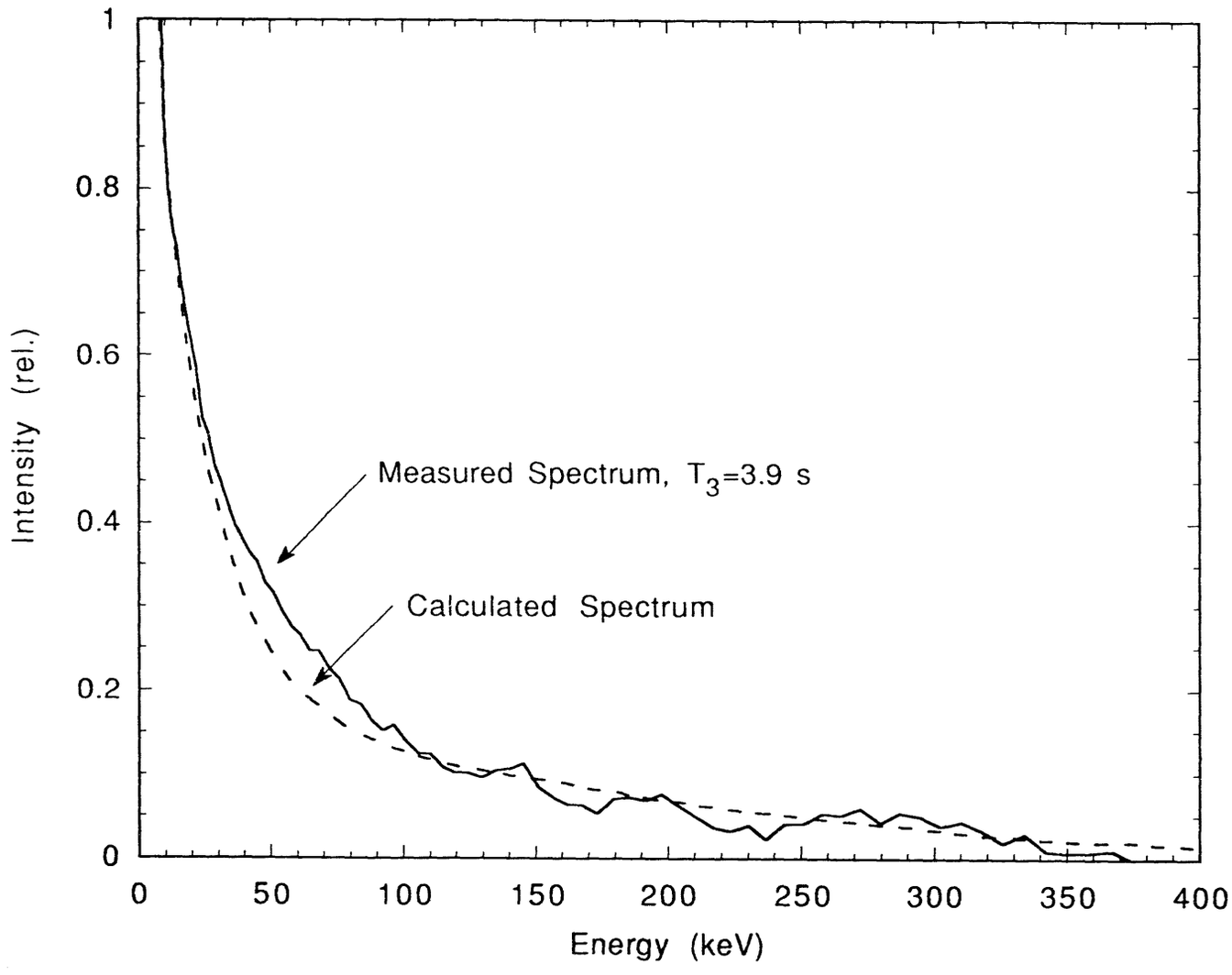
Intensity (rel.)
1
0.8
0.6
0.4
0.2
0
0
50
100
150
200
250
300
350
400
Energy (keV)
Measured Spectrum, T_3=3.9 s
Calculated Spectrum

Fig. 5

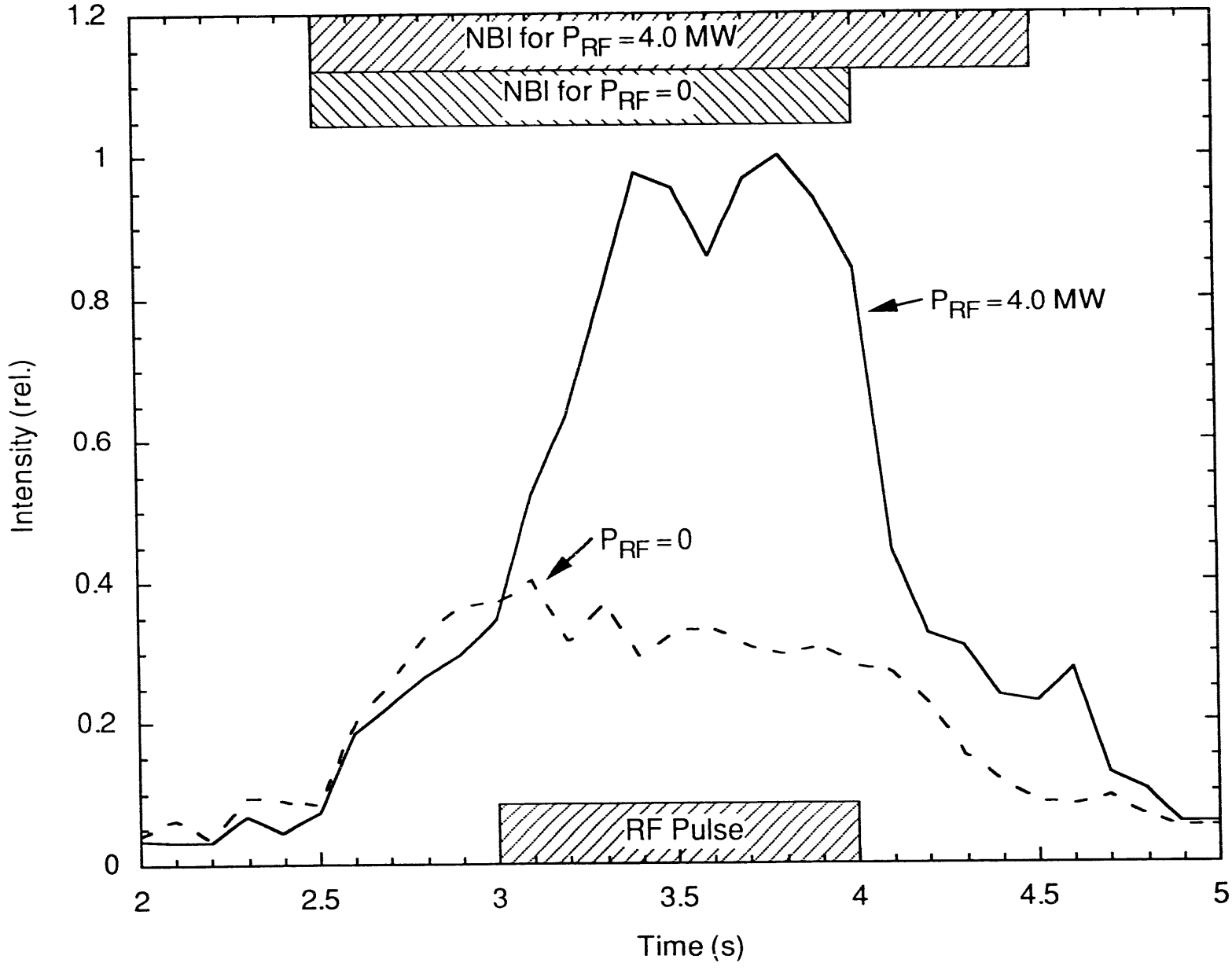
NBI for P_{RF} = 4.0 MW
NBI for P_{RF} = 0
P_{RF} = 4.0 MW
P_{RF} = 0
RF Pulse
Intensity (rel.)
Time (s)
1.2
1
0.8
0.6
0.4
0.2
0
2
2.5
3
3.5
4
4.5
5

Fig. 6

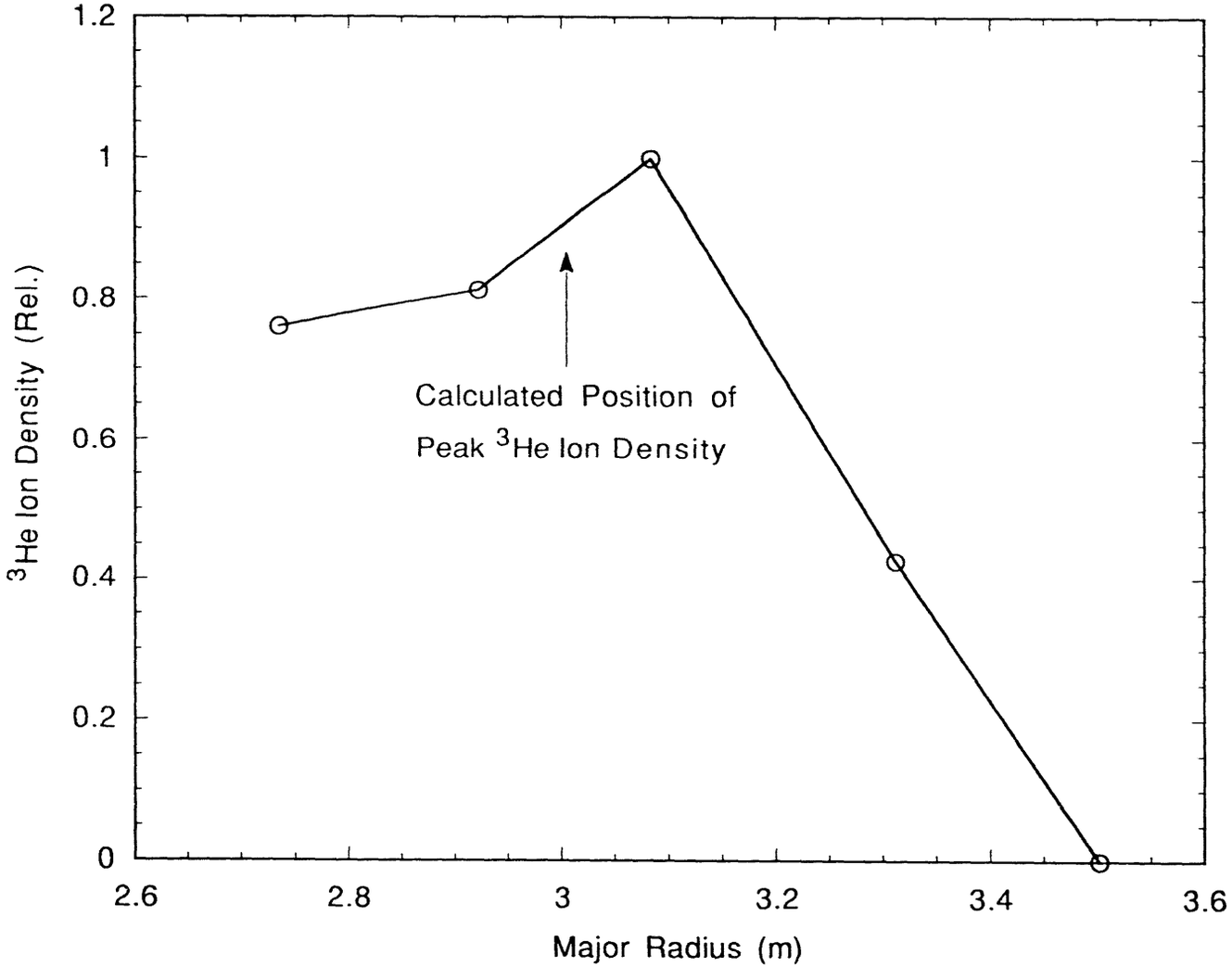
1.2
1
0.8
0.6
0.4
0.2
0
2.6
2.8
3
3.2
3.4
3.6
Major Radius (m)
^{3}He Ion Density (Rel.)
Calculated Position of
Peak ^{3}He Ion Density

Fig. 7

EXTERNAL DISTRIBUTION IN ADDITION TO UC-420

Dr. F. Paoloni, Univ. of Wollongong, AUSTRALIA
Prof. M.H. Brennan, Univ. of Sydney, AUSTRALIA
Plasma Research Lab., Australian Nat. Univ., AUSTRALIA
Prof. I.R. Jones, Flinders Univ, AUSTRALIA
Prof. F. Cap, Inst. for Theoretical Physics, AUSTRIA
Prof. M. Heindler, Institut für Theoretische Physik, AUSTRIA
Prof. M. Goossens, Astronomisch Instituut, BELGIUM
Ecole Royale Militaire, Lab. de Phy. Plasmas, BELGIUM
Commission-European, DG. XII-Fusion Prog., BELGIUM
Prof. R. Boucique, Rijksuniversiteit Gent, BELGIUM
Dr. P.H. Sakanaka, Instituto Fisica, BRAZIL
Prof. Dr. I.C. Nascimento, Instituto Fisica, Sao Paulo, BRAZIL
Instituto Nacional De Pesquisas Espaciais-INPE, BRAZIL
Documents Office, Atomic Energy of Canada Ltd., CANADA
Ms. M. Morin, CCFM/Tokamak de Varennes, CANADA
Dr. M.P. Bachynski, MPB Technologies, Inc., CANADA
Dr. H.M. Skarsgard, Univ. of Saskatchewan, CANADA
Prof. J. Teichmann, Univ. of Montreal, CANADA
Prof. S.R. Sreenivasan, Univ. of Calgary, CANADA
Prof. T.W. Johnston, INRS-Energie, CANADA
Dr. R. Bolton, Centre canadien de fusion magnétique, CANADA
Dr. C.R. James,, Univ. of Alberta, CANADA
Dr. P. Lukác, Komenského Universzita, CZECHO-SLOVAKIA
The Librarian, Culham Laboratory, ENGLAND
Library, R61, Rutherford Appleton Laboratory, ENGLAND
Mrs. S.A. Hutchinson, JET Library, ENGLAND
Dr. S.C. Sharma, Univ. of South Pacific, FIJI ISLANDS
P. Mähönen, Univ. of Helsinki, FINLAND
Prof. M.N. Bussac, Ecole Polytechnique,, FRANCE
C. Mouttet, Lab. de Physique des Milieux Ionisés, FRANCE
J. Radet, CEN/CADARACHE - Bat 506, FRANCE
Prof. E. Economou, Univ. of Crete, GREECE
Ms. C. Rinni, Univ. of Ioannina, GREECE
Preprint Library, Hungarian Academy of Sci., HUNGARY
Dr. B. DasGupta, Saha Inst. of Nuclear Physics, INDIA
Dr. P. Kaw, Inst. for Plasma Research, INDIA
Dr. P. Rosenau, Israel Inst. of Technology, ISRAEL
Librarian, International Center for Theo Physics, ITALY
Miss C. De Palo, Associazione EURATOM-ENEA , ITALY
Dr. G. Grosso, Istituto di Fisica del Plasma, ITALY
Prof. G. Rostangni, Istituto Gas Ionizzati Del Cnr, ITALY
Dr. H. Yamato, Toshiba Res & Devel Center, JAPAN
Prof. I. Kawakami, Hiroshima Univ., JAPAN
Prof. K. Nishikawa, Hiroshima Univ., JAPAN
Librarian, Naka Fusion Research Establishment, JAERI, JAPAN
Director, Japan Atomic Energy Research Inst., JAPAN
Prof. S. Itoh, Kyushu Univ., JAPAN
Research Info. Ctr., National Instit. for Fusion Science, JAPAN
Prof. S. Tanaka, Kyoto Univ., JAPAN
Library, Kyoto Univ., JAPAN
Prof. N. Inoue, Univ. of Tokyo, JAPAN
Secretary, Plasma Section, Electrotechnical Lab., JAPAN
S. Mori, Technical Advisor, JAERI, JAPAN
Dr. O. Mitarai, Kumamoto Inst. of Technology, JAPAN
Dr. G.S. Lee, Korea Basic Sci. Ctr., KOREA
J. Hyeon-Sook, Korea Atomic Energy Research Inst., KOREA
D.I. Choi, The Korea Adv. Inst. of Sci. & Tech., KOREA
Prof. B.S. Liley, Univ. of Waikato, NEW ZEALAND
Inst of Physics, Chinese Acad Sci PEOPLE'S REP. OF CHINA
Library, Inst. of Plasma Physics, PEOPLE'S REP. OF CHINA
Tsinghua Univ. Library, PEOPLE'S REPUBLIC OF CHINA
Z. Li, S.W. Inst Physics, PEOPLE'S REPUBLIC OF CHINA
Prof. J.A.C. Cabral, Instituto Superior Tecnico, PORTUGAL
Prof. M.A. Hellberg, Univ. of Natal, S. AFRICA
Prof. D.E. Kim, Pohang Inst. of Sci. & Tech., SO. KOREA
Prof. C.I.E.M.A.T, Fusion Division Library, SPAIN
Dr. L. Stenflo, Univ. of UMEA, SWEDEN
Library, Royal Inst. of Technology, SWEDEN
Prof. H. Wilhelmson, Chalmers Univ. of Tech., SWEDEN
Centre Phys. Des Plasmas, Ecole Polytech, SWITZERLAND
Bibliotheek, Inst. Voor Plasma-Fysica, THE NETHERLANDS
Asst. Prof. Dr. S. Cakir, Middle East Tech. Univ., TURKEY
Dr. V.A. Glukhikh,Sci. Res. Inst. Electrophys I Apparatus, USSR
Dr. D.D. Ryutov, Siberian Branch of Academy of Sci., USSR
Dr. G.A. Eliseev, I.V. Kurchatov Inst., USSR
Librarian, The Ukr.SSR Academy of Sciences, USSR
Dr. L.M. Kovrizhnykh, Inst. of General Physics, USSR
Kernforschungsanlage GmbH, Zentralbibliothek, W. GERMANY
Bibliothek, Inst. Für Plasmaforschung, W. GERMANY
Prof. K. Schindler, Ruhr-Universität Bochum, W. GERMANY
Dr. F. Wagner, (ASDEX), Max-Planck-Institut, W. GERMANY
Librarian, Max-Planck-Institut, W. GERMANY

DATE
FILMED
12/20/93

END